Ehmt1 forebrain haploinsufficiency leads to impaired memory, sensory gating and information processing

Brittany A. Davis[1], François David[1], Ciara O'Regan[2], Manal A. Adam[2], Adrian J. Harwood[1], Vincenzo Crunelli[1] & Anthony R. Isles[2*]

[1]Neuroscience and Mental Health Research Institute and School of Biosciences, Cardiff University, Cardiff, UK

[2]MRC Centre for Neuropsychiatric Genetics and Genomics, School of Medicine, Cardiff University Cardiff, UK

*Correspondence to: Anthony Isles, MRC CNGG, Cardiff University, Hadyn Ellis Building, Maindy Road, Cardiff, CF24 4HQ, UK; Email: *IslesAR1@cardiff.ac.uk*; Tel. ++44(0)2920688467

ABSTRACT

Regulators of chromatin dynamics and transcription are increasingly implicated in the aetiology of neurodevelopmental disorders (NDDs). Haploinsufficiency of *EHMT1*, encoding a histone methyl-transferase, is associated with several NDDs, including Kleefstra syndrome, developmental delay and autism spectrum disorder. In order to examine the brain role of *EHMT1* we developed and tested a forebrain specific conditional *Ehmt1* deletion mouse model (*Ehmt1*$^{D6Cre/+}$). We find that *Ehmt1*$^{D6Cre/+}$ mice have a number of abnormalities in spontaneous behaviours such as activity and anxiety. Of greater relevance to NDDs, we also show that *Ehmt1*$^{D6Cre/+}$ mice have deficits in information processing, evidenced by abnormal sensory-motor gating, a complete absence of object recognition memory and a reduced magnitude of auditory evoked potentials in both paired-pulse inhibition and mismatch negativity (MMN). The electrophysiological experiments show that differences in magnitude response to auditory stimulus were associated with marked reductions in total and evoked beta- and gamma-band oscillatory activity, as well as significant reductions in phase synchronisation. The pattern of electrophysiological deficits in *Ehmt1*$^{D6Cre/+}$matches those seen in control mice following administration of the selective NMDA antagonist, ketamine. This, coupled with reduction of *Grin1* mRNA expression in *Ehmt1*$^{D6Cre/+}$ hippocampus, suggests that *Ehmt1* haploinsufficiency may lead to disruption in NMDA-R. Taken together, these data indicate that reduced *Ehmt1* dosage during brain development leads to abnormal forebrain circuitry formation, which in turn results in profound information processing deficits. Such information processing deficits are likely paramount to our understanding of the cognitive and neurological dysfunctions shared across the NDDs associated with *EHMT1* haploinsufficiency.

Keywords: Neurodevelopmental disorders; mouse model; startle and PPI; auditory event related potentials; forebrain function; NMDA-R hypofunction

INTRODUCTION

Post-translational modifiers of histone proteins influence chromatin dynamics and transcriptional regulation throughout development and are essential for the highly choreographed processes of lineage commitment and differentiation during neurodevelopment [1, 2]. Perhaps unsurprisingly, exome sequencing studies and pathway analyses of genome wide association studies implicate genes encoding chromatin and transcriptional regulators in the aetiology of autism spectrum disorders [3, 4], schizophrenia [5] and severe developmental disorders [6, 7]. One such gene, implicated in several neurodevelopmental and neuropsychiatric disorders [8], is *EHMT1,* which encodes the histone H3 lysine 9 mono- and di-methyltransferase G9a-like protein (GLP).

Haploinsufficiency of *EHMT1* is the primary cause of the 9q34 subtelomeric-deletion syndrome, also known as Kleefstra Syndrome [9, 10], a condition associated with intellectual disabilities, epilepsy, childhood hypotonia, facial dysmorphism, microcephaly, delays in reaching developmental milestones and behavioural problems such as aggressive outbursts and hypoactivity. Furthermore, analysis of CNVs [11] and a large exome sequencing study [7] have linked *de novo* mutations affecting *EHMT1* to severe developmental delay more generally. Finally, CNVs spanning *EHMT1* have also been associated with autism spectrum disorder [12] and schizophrenia [13]. The severity and breadth of neurodevelopmental and neuropsychiatric phenotypes associated with changes in *EHMT1* dosage are a strong indication of the central importance of this gene to brain development and function [8].

EHMT1 is primarily associated with repressive transcriptional states [14] and is found to dynamically regulate diverse neural processes, from contextual fear memory [15, 16], addiction and stress [17-19] and most recently, synaptic scaling [20]. However, current animal models of *Ehmt1*-loss exemplify the limitations that can arise from interspecies modeling of gene function. The importance of *Ehmt1* expression throughout peripheral as well as cerebral tissue during development limit interpretation of phenotypes in constitutive heterozygous knockout mice. *Ehmt1*$^{+/-}$ mice show reduction in activity and exploration, and increased anxiety; but also reduced muscular strength and increased weight [21]. This combination of phenotypes presents confounding interpretations for the examination of behavioral and cognitive function. In contrast, an *Ehmt1*$^{-/-(\text{CamkII-cre})}$ mouse [22] has a greater degree of anatomical specificity, but only models

postnatal consequences of gene loss. Meanwhile, previous studies show *Ehmt1* is highly expressed in embryonic brain, with adult expression only in restricted areas [10], suggesting postnatal ablation is unlikely to recapitulate the full range of disease-specific pathologies.

In order to reduce anatomical complexity and allow a more precise focus on the impact of *Ehmt1* haploinsufficiency during development, on later behavioural and neurophysiological parameters, we generated a forebrain-specific *Ehmt1* knockout mouse. Cre recombination was driven under the D6 promoter of the *Dach1* gene limiting *Ehmt1* heterozygous deletion to the forebrain, starting at embryonic stage 10.5 in the cortical vesicles [23, 24]. Here we show that *Ehmt1*$^{D6Cre/+}$ mice recapitulate behavioural endophenotypes shared across the spectra of neurodevelopmental disorders associated with *Ehmt1* mutations, including hypoactivity, altered anxiety and memory deficiency. In addition, information processing and gating abnormalities are identified with decreases in sensorimotor and auditory gating and a reduction in the magnitude of auditory evoked potentials in paired-pulse inhibition and MMN, provide both behavioural and electrophysiological evidence of impairment in the *Ehmt1*$^{D6Cre/+}$ mice. Gene expression data and pharmacological manipulation are supportive of an NMDA-R hypofunction in *Ehmt1*$^{D6Cre/+}$ adult mouse. Taken together these data suggest that correct developmental expression of *Ehmt1* is required for normal brain and behaviour. Loss of gene function leads to abnormal circuit formation, information processing deficits and disruptions in gamma and beta band activity, which in turn may underpin the global deficits seen in those disorders associated with *EHMT1* haploinsufficiency.

RESULTS

Generation of *Ehmt1*$^{D6\ Cre/+}$ mouse

Expression analysis in wild-type mice followed that of previous studies [10], showing high levels of Ehmt1 throughout embryonic brain development and into the early post-natal period (Figure 1A), with peaks in Ehmt1 expression at E14.5 and P7. Expression levels were the lowest in the adult brain. G9a expression matched that of Ehmt1 up until E14.5, where after Ehmt1 decreases whilst G9a remains highly expressed. Ehmt1 expression is matched closely by the overall pattern of H3K9me2 throughout development (Figure 1A).

Having confirmed that Ehmt1 expression was highest during embryonic brain development, we generated a mouse model that incorporates the temporal peak of expression with anatomical forebrain-specificity. Crossing an existing *Ehmt1*$^{Flp/Flp}$ line [22] with a *D6-Cre* line [23, 24] successfully deleted *Ehmt1* exon 23 in frontal cortex and hippocampal samples, but not cerebellum of *Ehmt1*$^{D6Cre/+}$ mice (Supplementary Methods and Supplementary Figure 1). *Ehmt1*$^{D6Cre/+}$ mice were present in normal Mendelian ratios and demonstrated normal weight throughout development (data not shown).

Normal motor function but reduced activity levels in the *Ehmt1*$^{D6Cre/+}$ mouse

Basal activity levels in *Ehmt1*$^{D6Cre/+}$ mice were significantly reduced relative to *Ehmt1*$^{flp/+}$ mice as measured over five consecutive 2-hour sessions. Thus, analysis of infrared beam breaks across the first 2-hour session broken into 5-minute bin showed the canonical general reduction in over time (Figure 1B; ANOVA, main effect of BIN, $F_{10.46,282.28=}$29.87, p<0.001) but also a main effect of GENOTYPE ($F_{27,1=}$5.35, p=0.03). However, there was no interaction between BIN and GENOTYPE ($F_{10.46,\ 282.28=}$1.09, p=0.36), suggesting *Ehmt1*$^{D6Cre/+}$ mice habituated as normal, but were generally hypoactive. Analysis of total beam breaks showed an average 50% reduction in activity generally between the first (days 1) and last sessions (day 5) (Figure 1C: ANOVA, main effect of DAY, $F_{1,27}$=25.24, p=0.001) with a lower level of activity in *Ehmt1*$^{D6Cre/+}$ mice (main effect of GENOTYPE, $F_{1,27=}$7.38, p=0.01). Again there was no interaction between DAY and GENTOYPE ($F_{1,27}$=0.25, p=0.62).

Reduced activity levels in *Ehmt1*$^{D6Cre/+}$ mice were not due to any gross deficits in motoric competence however. Training on the rotarod test indicated normal learning with repeated sessions, with latency to fall reducing across training sessions (ANOVA, main effect of SESSION, $F_{5,130}$=21.33, p<0.001), but there was no difference in GENOTYPE ($F_{1,26}$=0.12, p=0.73) and no interaction between training SESSION and GENOTYPE ($F_{5,130}$=0.67, p=0.65). Moreover, in an accelerating rotarod probe test of motor coordination, latency to fall decreased as the speed increased (ANOVA, main effect of SPEED, $F_{4,104}$=38.38, p<0.001), but there was no difference between GENOTYPE ($F_{1,\ 26}$=0.67, p=0.42) or interaction between SPEED and GENOTYPE ($F_{4,104}$=0.65, p =0.63).

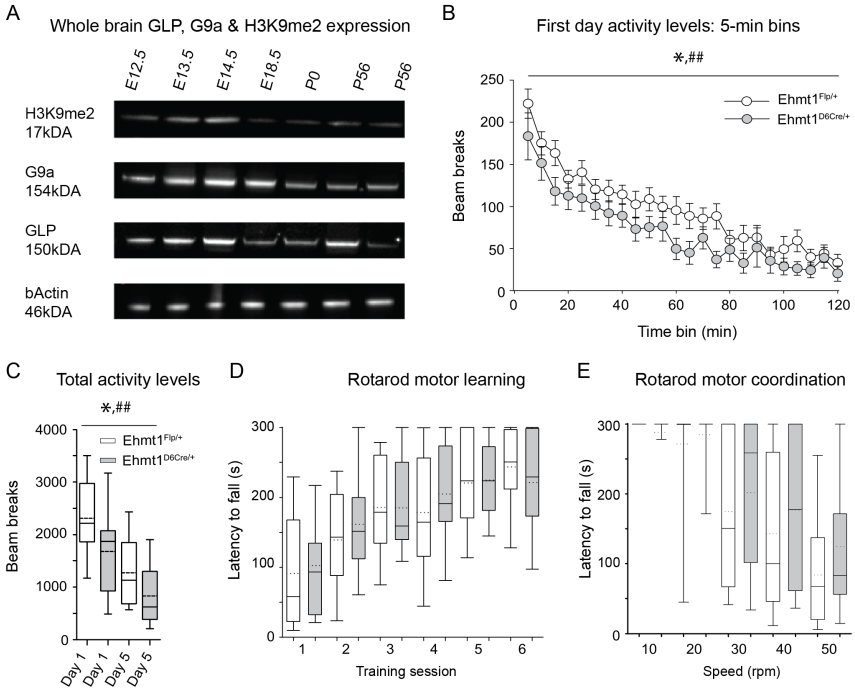

Figure 1. GLP protein expression & motor learning and coordination

A) Protein expression of GLP, G9a and H3K9me2 during mouse development. **B**) Activity levels across the first 2-hour session reduce over time but are generally lower in *Ehmt1*$^{D6Cre/+}$ mice. **C)** Total numbers of total beam breaks are generally lower on the first (day 1) compared to the last (day 5) consecutive daily 2-hour session. *Ehmt1*$^{D6Cre/+}$ consistently make fewer beam breaks, indicating a general hypoactivity phenotype. **D)** All animals improve motor ability on the rotarod as evidenced by an increase in latency to fall across 6 training sessions. There was no also difference in genotype during training **E)** In a probe test where rotarod speed accelerated throughout the session there was a general decrease in the latency to fall as the speed increased, but again no difference between genotypes suggesting *Ehmt1*$^{D6Cre/+}$ mice do not a have a motor deficit compared to *Ehmt1*$^{Flp/+}$ controls. Data are mean ±SEM, or box-plots showing median (solid line), mean (dashed line) and 10th, 25th and 75th and 90th percentiles. * represents main effect of GENOTYPE p<0.05; ## represents main effect of within-subject factor (BIN or DAY).

Reduced anxiety and greater novelty-exploration in *Ehmt1*$^{D6Cre/+}$ mouse

A number of measures, across three separate tests, indicated that *Ehmt1*$^{D6Cre/+}$ mice have a reduced anxiety phenotype. On the elevated plus maze (EPM), *Ehmt1*$^{D6Cre/+}$ mice made statistically equivalent entries (Figure 2A; $t_{1,26}$=-1.52, p=0.14) but spent on average twice as long as *Ehmt1*$^{Flp/+}$ cage-mates in the open-arm section (Figure 2B; t_{26}=-2.08, p=0.04). In the open field (OF), *Ehmt1*$^{D6Cre/+}$ made 25% more entries in the inner zone (Figure 2C; t_{26}= -3.21,

p=0.004), although time in the inner zone was not significantly different to *Ehmt1*$^{Flp/+}$ cage-mates (Figure 2D; t_{26}=-1.86, p=0.07).

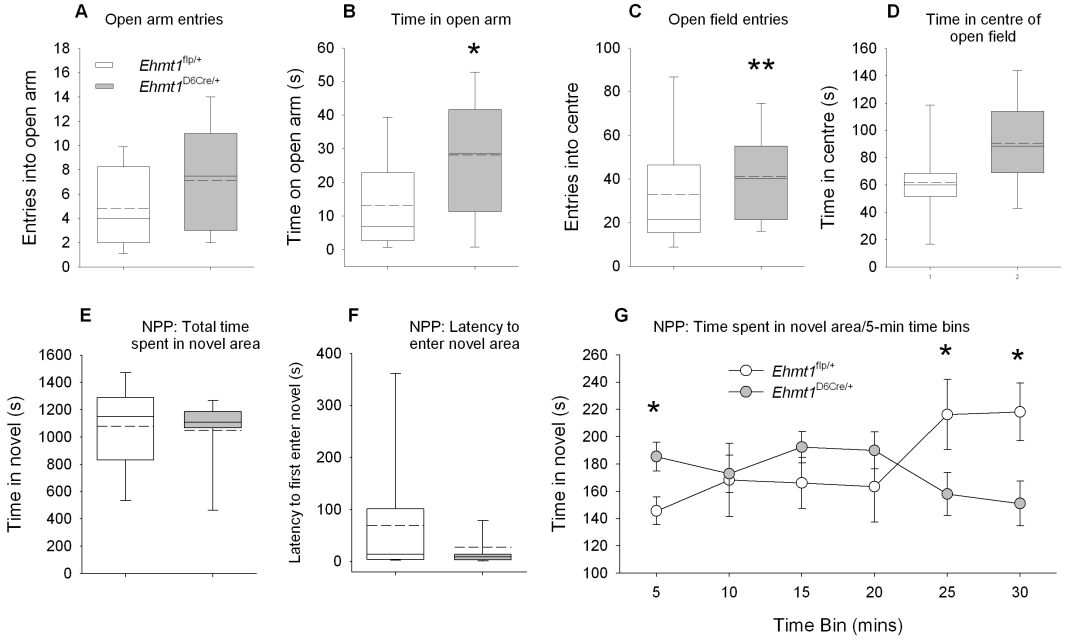

Figure 2. Novelty exploration and anxiety-related measurements

A) On the EPM, *Ehmt1*$^{D6Cre/+}$ show a trend for increased entries into open arm, but this is not statistically different from controls. **B**) However, on average *Ehmt1*$^{D6Cre/+}$ mice spent twice as much time in the open-arm section of the maze as *Ehmt1*$^{Flp/+}$. This was supported by data from the OF test (**C**) where *Ehmt1*$^{D6Cre/+}$ made 25% more entries in the inner zone than *Ehmt1*$^{Flp/+}$ controls. Although generally higher in *Ehmt1*$^{D6Cre/+}$ mice time spent in the centre of the OF (**D**) this did not reach significance. **E**) Willingness to explore a novel environment was measured in the NPP. Although the total time spent (**E**) in to the novel chamber of NPP test was not statistically different between genotypes, the pattern of latencies to first enter the novel chamber (**F**) suggested that *Ehmt1*$^{D6Cre/+}$ mice were generally quicker than *Ehmt1*$^{Flp/+}$ controls. Binned analysis of the NPP (**G**) revealed that *Ehmt1*$^{D6Cre/+}$ mice spent significantly more time in first 5min bin exploring the novel chamber, whereas the *Ehmt1*$^{flp/+}$ controls preferred habituated chamber. Conversely, in the last 5min bin controls spent significantly greater time exploring the novel chamber. Data shown is mean ±SEM, or box-plots showing median (solid line), mean (dashed line) and 10th, 25th and 75th and 90th percentiles; data shown is. * represents main effect of GENOTYPE p<0.05; ** p<0.01.

Another aspect of anxiety is the willingness to explore novelty, and to test this we used a novelty place preference (NPP) task. Both *Ehmt1*$^{D6Cre/+}$ and *Ehmt1*$^{Flp/+}$ mice spent an equivalent length of time in the novel chamber (Figure 2E; t_{25}=0.25, p=0.81). Although also not statistically different (t_{25} =1.16, p=0.26), a reduced latency to explore (Figure 2F) suggested a skewing of the time spent throughout the trial for *Ehmt1*$^{D6Cre/+}$, warranting further analysis. In a binned analysis of

time spent in the novel chamber there was no main effect of GENOTYPE (Figure 2G; $F_{1,25}$=0.062, p=0.81), but there was an interaction between GENOTYPE and BIN ($F_{5,125}$=6.78, p=0.0001) suggesting a different pattern of behaviour throughout the NPP task. *Post hoc* analysis revealed that *Ehmt1*$^{D6Cre/+}$ mice spent greater than 50% of the first 5-minute bin exploring the novel chamber ($t_{26=}$-2.39, p=0.025), whereas *Ehmt1*$^{Flp/+}$ cage-mates preferred the habituated chamber. As the test progressed this behavior switched; in the last two 5-minute bins *Ehmt1*$^{Flp/+}$ mice preferred the novel chamber (t_{26}=2.44, p=0.02).

Impaired sensory-motor gating in *Ehmt1*$^{D6Cre/+}$ mouse

The acoustic startle response and pre-pulse inhibition (PPI) of this response, were used to examine sensory-motor function in the *Ehmt1*$^{D6Cre/+}$ mice. Over the course of six consecutive auditory pulse (120dB) startle trials, *Ehmt1*$^{D6Cre/+}$ mice had, on average, twice the startle response compared to *Ehmt1*$^{Flp/+}$ mice (Figure 3A; ANOVA, main effect of GENOTYPE, $F_{1,53}$=6.86, p=0.01). A significant interaction between GENOTYPE and TRIAL ($F_{3.87,201.0}$=2.48, p=0.03) indicated different patterns of startle reactivity and habituation relative to controls. *Post hoc* analysis revealed that there was an equivalent startle response to the initial trial between genotypes (p=0.68), but on average *Ehmt1*$^{D6Cre/+}$ mice showed a significantly enhanced startle response in all consecutive trials (trial 2, p=0.05; 3, p=0.01; 4, p=0.001; 5, p=0.01; and 6, p=0.02).

PPI is examined by delivering a prepulse of 4, 8 and 16 dB prior to onset of the startle pulse. As expected, increasing the prepulse volume led to a linear increase in the inhibition of the startle in both groups (Figure 3B; ANOVA, main effect of PPI, $F_{1.49,80.35}$=73.26, p=0.001). However, there was a 20-40% PPI reduction in the *Ehmt1*$^{D6Cre/+}$ mice relative to *Ehmt1*$^{Flp/+}$ cage-mates (Figure 3B; ANOVA main effect of GENOTYPE, $F_{1,54}$=5.54, p=0.022), suggesting that, in addition to an enhanced startle response, the mutant mice were also impaired in the normal PPI response.

Impaired novel object recognition in *Ehmt1*$^{D6Cre/+}$ mouse

The novel object recognition (NOR) task takes advantage of the preference of rodents to attend to new objects in their environment as a means for testing declarative memory [25]. Here, two inter-trial intervals were used: half of the cohort was examined following a 15-minute delay between the initial object exposure and the test trial, and half the cohort was examined after a 90-minute delay. In the test phase, as expected the *Ehmt1*$^{Flp/+}$ control mice explored the novel object

significantly more than chance (50%) in both the 15-minute and 90-minute retention trials (Figure 3C; Kolmogorov Smirnov test (KS), 15min, 60%, p=0. 02; 90min retention trial, 67%, p=0.002). However, exploration of the novel object by *Ehmt1*$^{D6Cre/+}$ mice was not significantly above chance, at either 15min (52%, $p=0.97$), or 90 min retention trial (50%, p=0.44). This difference at test was not due to difference in the overall time spent exploring objects during the habituation phase (ANOVA, no main effect of GENOTYPE, $F_{29,1}$=0.31, p=0.86; data not shown).

Figure 3. Sensorimotor gating & novel object recognition

A) The startle response after 6 consecutive 120dB pulse stimulations show *Ehmt1*$^{D6Cre/+}$ mice had a significantly higher overall maximum startle response in all trials. **B**) Inhibition of the startle response following a prepulse tone generally increased with the increasing volume of the prepulse as expected. However, *Ehmt1*$^{D6Cre/+}$ mice displayed a 20-40% reduction in PPI of startle relative to *Ehmt1*$^{Flp/+}$ controls. **C**) In both the 15-minute and 90-minute retention tests of the NOR task *Ehmt1*$^{Flp/+}$ control mice explored the novel object more than chance. However, exploration of the novel object by *Ehmt1*$^{D6Cre/+}$ mice was not significantly above chance, for either the 15- or 90-minute retention trials indicating a deficit in declarative memory. Data are mean ±SEM or box-plots showing median (solid line), mean (dashed line) and 10th, 25th and 75th and 90th percentiles (dots represent 5th and 95th percentile). * represents main effect of GENOTYPE p<0.05; ** p<0.01; ## represents main effect of PREPULSE.

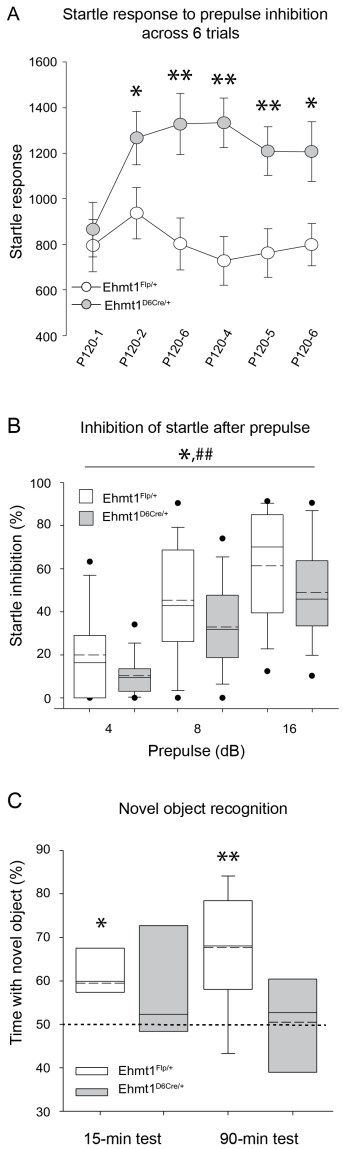

Electrophysiological measurements of paired pulse AEPs

In order to gain an insight into the neural changes underpinning behavioural deficits in sensory-motor gating seen in *Ehmt1*$^{D6Cre/+}$ mice we used EEG to measure auditory evoked potentials (AEPs). AEPs are voltage fluctuations time-locked to an auditory event [26]. We used a paired pulse paradigm in which two pulses were delivered back-to-back with a 500ms interval between the first stimulus (S1) and the second stimulus (S2) (Figure 4A). The grand average waveforms show a stereotypic maximal positive deflection (P1) and maximal negative deflection (N1) (Figure 4 B1). *Ehmt1*$^{D6Cre/+}$ mice had a nearly two-fold lower N1 amplitude response after the S1 (Figure 4B1) but not after S2 (Figure 4B2). Additionally, *Ehmt1*$^{D6Cre/+}$ mice had a significant reduction in the S2/S1 ratio for the N1 component (Wilcoxon, ranksum=64, p=0.018), what is considered an electrophysiological measurement of sensory gating (Figure 4C). During peak activation of the paired pulse experiment we observed an increase in total power across high frequency bands from 10-100Hz in both groups of mice (Figure 4D1 and D2). The difference time-frequency plot and the permutation test between *Ehmt1*$^{D6Cre/+}$ and *Ehmt1*$^{Flp/+}$ control mice however, revealed that the distributed peak that occurred approximately 40ms after the S1 pulse, a time corresponding with the N1, was significantly greater in the beta (13-30Hz) and gamma (30-70Hz) frequency bands in the *Ehmt1*$^{Flp/+}$ control mice (Figure 4G1 and G2). The late (>200ms after the S1 pulse) decrease in the delta frequency band (~4Hz) prominent in *Ehmt1*$^{Flp/+}$ (Figure 4D1-G1) was not different from *Ehmt1*$^{D6Cre/+}$ (Figure 4G2).

Measurements of evoked power, EEG power which is phase-locked with the event onset across trials, demonstrated increases in the delta (~4hz), beta (13-30Hz) and low gamma (here ~40Hz) band responses in both groups of mice approximately ~30-50 ms after the S1 (Figure 4E1 and E2). Again, permutation tests revealed a reduction in evoked power in *Ehmt1*$^{D6Cre/+}$ mice after both the S1 and ~40ms after the S2 pulse (Figure 4H1 and H2). In complement, we measured the phase locking factor (PLF), which provide a measurement of trial-to-trial reliability across the frequency domain [27]. To extract the PLF, magnitude information is transformed to 1 and averaged so that the phase angle with respect to event onset is extracted [28]. Values between zero and one are obtained, in which one reflects perfect synchrony of phase angles across trials. *Ehmt1*$^{D6Cre/+}$ mice did not show PLF values above .17 at any point, while control mice show nearly two-fold PLF synchrony (+.25) at ~40ms post-S1 pulse, between ~20-40Hz. Overall *Ehmt1*$^{D6Cre/+}$mice demonstrated reduced PLF (Figure 4F1 and F2).

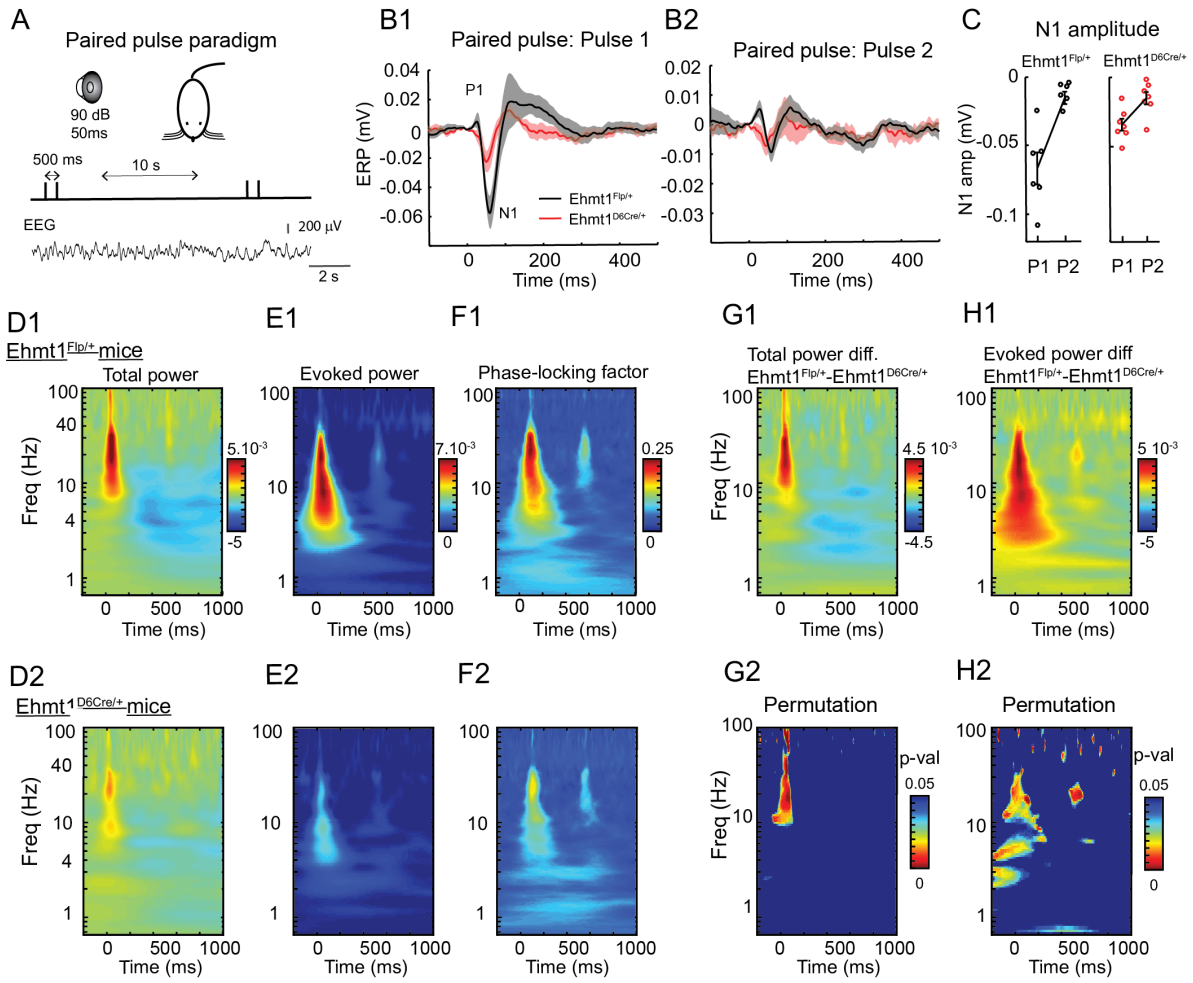

Figure 4. AEP paired pulse measurements

A) Schematic showing the paired pulse stimulus paradigm. **B1**) Grand average ERP waveform after pulse 1 (S1) in *Ehmt1*$^{D6Cre/+}$(red) *and Ehmt1*$^{Flp/+}$ (black). The P1 and N1 components are indicated on the waveform. **B2**) The waveforms for pulse 2 (S2); **C)** N1 amplitude for *Ehmt1*$^{D6Cre/+}$ mice (left) and *Ehmt1*$^{Flp/+}$ mice (right). **D1 & D2)** Normalized total power (in time-frequency plot) of both S1 (time 0) and S2 (time 500ms) for *Ehmt1*$^{Flp/+}$ (D1) and *Ehmt1*$^{D6Cre/+}$ (D2). Note the early increase in the beta/gamma range (10-100Hz) and the late decrease in the delta range (~4Hz) and the reduction of both components in the *Ehmt1*$^{D6Cre/+}$. **E1 & E2)** Evoked power time-frequency plots for the same data set; **F1 & F2)** Phase locking factor for the same data set; **G1)** Difference of total power between *Ehmt1*$^{Flp/+}$ and *Ehmt1*$^{D6Cre/+}$. **G2)** Statistical significance heat map based on permutation tests of total power are indicated by the colour scale (p-value < 0.05); **H1)** Difference of evoked power between *Ehmt1*$^{Flp/+}$ and *Ehmt1*$^{D6Cre/+}$ mice; **H2)** Statistical significance between evoked power of *Ehmt1*$^{Flp/+}$ and *Ehmt1*$^{D6Cre/+}$ mice (spurious spots above 50Hz are due to occasional 50Hz noise contamination in some of the recordings). Data shown is mean ±SEM.

Electrophysiological measurements of Mismatched Negativity AEPs

The Mismatch Negativity (MMN) response is elicited when a qualitative feature of the stimulus does not match the pattern in a previous series [29] (Figure 5A). One core feature of MMN is the importance of NMDA receptor function. For instance, non-competitive NMDA antagonists, like ketamine and the selective antagonist of the NR2B NMDA subunit, CP-101,606 reduce MMN amplitude [30], the level of which predicts the magnitude of psychotic experiences in response to these drugs [31]. Therefore, in order to probe this function further here, mice were given either saline or 10mg/kg of ketamine prior to the MMN test.

In saline treated animals there was a difference between *Ehmt1*$^{\mathrm{D6Cre/+}}$ and *Ehmt1*$^{Flp/+}$ control mice in response to the deviant pulse (Figures 5C-D) as indicated by analysis of the N1 amplitude that showed an interaction between GENOTYPE and PULSE (repeated measures ANOVA, $F_{1,8}$=12.70, p=0.007). In the standard pulse condition *Ehmt1*$^{Flp/+}$ control mice, amplitude corresponded to an increase in ~10-40Hz evoked potential approximately 30-50ms post-stimulus (Figure. 5C1-C2). In the deviant pulse condition, *Ehmt1*$^{Flp/+}$ mice not only show an increase in ~10-40Hz evoked potential, but also one with greater peak latency, at 40-70ms post-stimulus (Figure 5C2). In contrast, *Ehmt1*$^{\mathrm{D6Cre/+}}$ mice treated with saline showed no pattern of change in the amplitude response for either standard or deviant pulses.

However, following ketamine administration, the difference in the N1 amplitude between the standard and deviant pulse was absent for both genotypes (Figure 5B and D), as indicated by a lack of interaction between GENOTYPE and PULSE (repeated measures ANOVA, $F_{1,7}$=0.011, p=0.921). Further analysis underlined this finding. Permutation tests after saline administration for the deviant-only condition demonstrates a difference between *Ehmt1*$^{Flp/+}$ controls and *Ehmt1*$^{\mathrm{D6Cre/+}}$ wavelet transforms, at 30Hz between 50-80ms post-stimulus (Figure 5E1), driven by the higher amplitude response in the *Ehmt1*$^{Flp/+}$ control mice. In contrast, after ketamine administration the difference in deviant response between *Ehmt1*$^{Flp/+}$ controls and *Ehmt1*$^{\mathrm{D6Cre/+}}$ mice was abolished (Figure 5E2).

Altered NMDA-receptor expression in *Ehmt1*$^{\mathrm{D6cre/+}}$ mutant mice

In light of similarity in basal *Ehmt1*$^{\mathrm{D6Cre/+}}$ electrophysiological phenotype and the electrophysiological phenotype in *Ehmt1*$^{Flp/+}$ control mice following ketamine administration, we assessed the NMDA system in *Ehmt1*$^{\mathrm{D6Cre/+}}$ mice. RT qPCR was used to examine the mRNA

levels of NMDA-R subunits *Grin1*, *Grin2a*, *Grin2b* and *Grin2c* in the adult hippocampus. Expression of *Grin1*, the gene encoding NMDA NR1 subunit, was significantly reduced by 40% on average in *Ehmt1*$^{D6cre/+}$ mice (Figure 5F; p=0.02). No difference was seen in *Grin2a* (p=0.34), *Grin2b* (p=0.30), or *Grin2c* (p=0.5) expression.

DISCUSSION

Recent studies in human genomics strongly implicate a number of genes found to regulate chromatin dynamics in the etiology of neurodevelopmental disorders from developmental delays [6], to autism spectrum disorders [3, 4], and schizophrenia [5]. *EHMT1* is one such gene, associated with both neurodevelopmental and neuropsychiatric disorders. Here we developed and tested a conditional *Ehmt1* mutant mouse model in order to bypass confounding effects of non-CNS disruption. This model allowed us to interrogate the consequences of developmental haploinsufficiency of this gene, specifically in the forebrain. We found that *Ehmt1*$^{D6Cre/+}$ mice have memory impairments, reduced anxiety and activity levels, and sensorimotor and auditory gating deficits. *Ehmt1*$^{D6Cre/+}$ mice also showed a number of abnormalities in electrophysiological measurements including a reduced magnitude of AEPs after paired-pulse inhibition and MMN tasks, reduced evoked and total power in high frequency bands, and reduce PLF. These data highlight the importance of correct *EHMT1* dosage in forebrain structures throughout neurodevelopment.

Ehmt1$^{D6Cre/+}$ mice were generally hypoactive and displayed decreased anxiety across a number of tests. These findings were not confounded by impaired motor competence, nor indeed did they confound one-another, as decreased anxiety measures on the EPM and OF are normally associated with increased activity levels [32]. These findings are consistent with previous studies of constitutive and/or conditional (CamkII-cre) *Ehmt1* knockout models [22, 33]. Furthermore our data suggest a robustness of effect of *Ehmt1* on spontaneous behaviour, which in turn underlies both the reproducibility of *Ehmt1* disruption and the validity of the *Ehmt1*$^{D6Cre/+}$ model, as well as the importance of forebrain-specific *Ehmt1* expression in aetiology of these phenotypes.

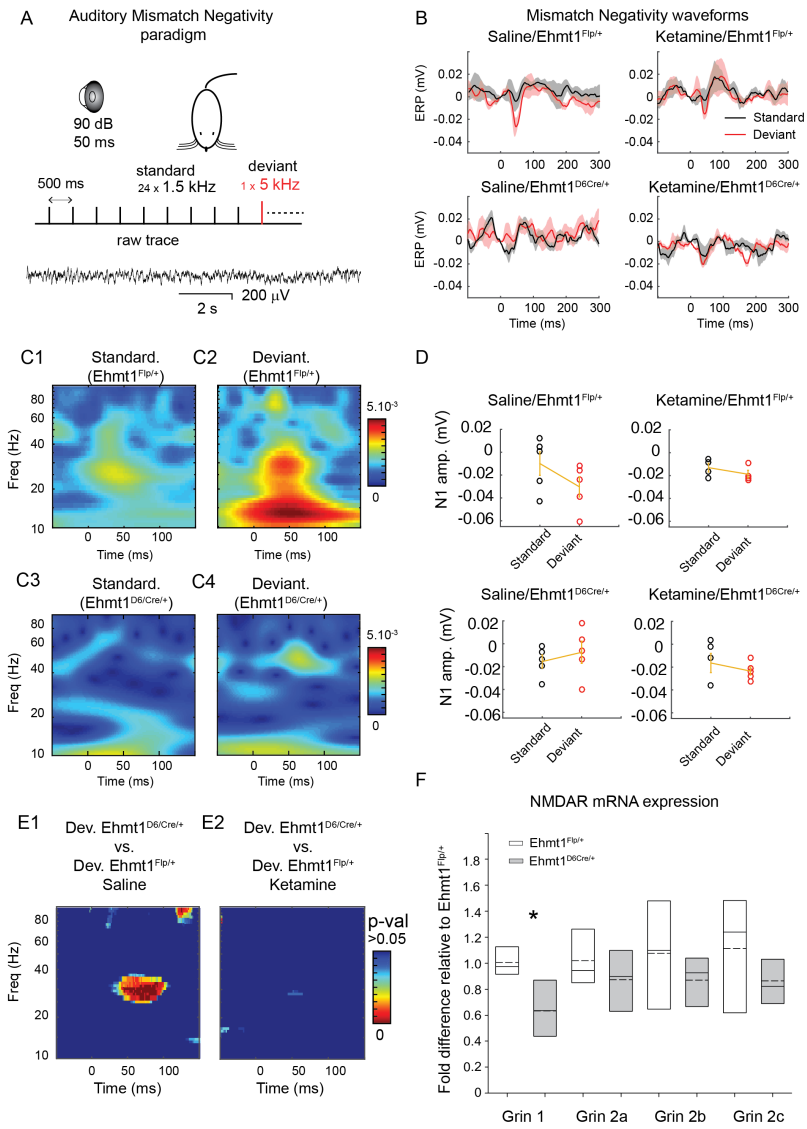

Figure 5. AEP mismatch negativity phenotypes & NMDA mRNA expression

A) Mismatch negativity stimulus **B)** Grand average ERP waveforms (shaded areas) after the saline or ketamine (left and right columns respectively) conditions in the in *Ehmt1*$^{Flp/+}$ and *Ehmt1*$^{D6Cre/+}$ (1st and 2nd row respectively), for the deviant (red) and standard (black) tone for each condition. **C1 & C2)** Time-frequency plot of evoked power for the standard (left) and deviant (right) pulse in *Ehmt1*$^{Flp/+}$ mice after saline injection; **C3 & C4)** Time-frequency plot of evoked power for the standard (left) and deviant (right) pulse in *Ehmt1*$^{D6Cre/+}$mice following saline injection. **D)** N1 amplitude peak amplitude corresponding to each condition. **E1)** Permutation test showing heat map of *p*-values for the difference of distribution between deviant tone maps of saline treated *Ehmt1*$^{Flp/+}$ (C2) and *Ehmt1*$^{D6Cre/+}$ (C4) (see colour scale). **E2**) Permutation test showing heat map of *p*-values for the difference of distribution between deviant tone maps of ketamine treated *Ehmt1*$^{Flp/+}$ (C2) and *Ehmt1*$^{D6Cre/+}$ (C4) (see colour scale). **F)** NMDA subunit mRNA expression in hippocampal samples. Data shown is mean ±SEM.

EHMT1 is a risk gene associated with a number of neurodevelopmental and psychiatric disorders [8], thus it was important for this work to focus not only on translational phenotypes but those that overlap traditional diagnostic boundaries. Several prominent features shared by these disorders are associated with deficits in attention and gate or filtering out intrusive stimuli [34-37]. Behaviorally, the *Ehmt1*$^{D6Cre/+}$ mice showed evidence of this in an acoustic startle test. Sensory motor gating deficits were manifest by both a greatly enhanced acoustic startle response, and a decreased pre-pulse inhibition of startle. We explored this further by examining electrophysiological measures of gating. *Ehmt1*$^{D6Cre/+}$ had reduced N1 amplitude in response to stimulus 1 (S1). Furthermore, *Ehmt1*$^{D6Cre/+}$ mice had a significant reduction in the S2/S1 ratio for the N1 component, an electrophysiological correlate of sensory gating.

Information-processing deficits are another common phenotype associated with *EHMT1* risk populations. Accordingly, *Ehmt1*$^{D6Cre/+}$ mice were examined on their performance in the NOR task, a paradigm where an animal's ability to remember a previously encountered object is indicated by an increased willingness to explore the novel object over the familiar object. The *Ehmt1*$^{D6Cre/+}$ mice showed no evidence of novel object recognition, even with only a 15-minute interval after habituation. Importantly, this was not due to reduced interest in exploration or exposure to the familiar object, as time spent in exploration was equivalent across *Ehmt1*$^{Flp/+}$ control and *Ehmt1*$^{D6Cre/+}$ mutant mice.

Further, electrophysiological evidence of information-processing deficits in the *Ehmt1*$^{D6Cre/+}$ mice was provided by the reduced response in a mismatch negativity(MMN) paradigm . The decreased amplitude responses in these AEP measurements meanwhile corresponded to significant reductions in total and evoked power in high frequency bands. Such reductions may be particularly insightful, as numerous studies report disruptions in gamma-band activity across neurodevelopment [35, 38], neuropsychiatric [39] and neurodegenerative diseases [40]. Whether reduced gamma activity is actually directly associated with disease pathologies across these patient populations remains largely unknown. Recently however, reductions in gamma-band activity were found to precede the onset of plaque formations and cognitive decline in a mouse model of Alzheimer's disease. Meanwhile the stimulation of fast-spiking interneurons in the gamma frequency range (~40Hz), a way to boost gamma-band activity [41], led to the reduction in the plaque forming amyloid isoforms and attenuated plaque load in ageing mice [40]. In a more functional assessment, the induction of long-term potentiation using high frequency

stimulation (~100Hz) was found to restore spine density and long-term memory in early stages of the disease in mice [42]. While these findings are specific to Alzheimers disease, they also confirm an important link between gamma synchrony and cognitive function exists [43]. Furthermore, we may find disruptions in high frequency oscillation patterns tightly correspond with the degree of cognitive impairment and range of pathologies across *EHMT1* risk populations.

The decreases in high frequency activity coupled with reduced *Grin1* mRNA are suggestive of overall disruptions in local connectivity and may hint to more global imbalances in excitation/inhibition (E/I). Such findings do corroborate previous reports showing changes in *Ehmt1*-mediated H3K9me2 levels dynamically regulate synaptic scaling, thus playing a direct role in the fine balance between excitation and inhibition at the level of individual neurons [20]. And indeed many of the *Ehmt1*$^{\mathrm{D6Cre/+}}$ mice phenotypes are markedly similar to *Grin1* mouse mutants [44]. The *Grin1*$^{neo\text{-}/\text{-}}$ mice and the *Grin1*^{Rgsc174} heterozygous mice both show novelty induced hyperactivity, increased stereotypy [45] and deficits in sensorimotor gating [46]. Mice with even subtle reductions in the NR1 receptor are found to have decreases in MMN [47], gamma-band disruptions and reduction in E/I balance [48]. Thus future investigation of the *Ehmt1* haploinsufficiency may benefit from further examination of the relationship between reductions in gamma-band activity and NMDA-hypofunction.

In summary, *Ehmt1*$^{\mathrm{D6Cre/+}}$ forebrain-specific haploinsufficiency produced deficits in sensory-gating and information processing. Behavioural evidence from explicit tests of sensorimotor gating and findings from a learning and memory task, suggest that *Ehmt1*$^{\mathrm{D6Cre/+}}$ mice do not attend to or process information in order to inform appropriate behavioural responses. Neural correlates of these abnormalities were further demonstrated using translational electrophysiological studies, which indicated deficits related to disruptions in local connectivity and NMDA function. Taken together these data suggest that correct developmental expression of *Ehmt1* is required for normal brain and behaviour in the adult mouse. Finally *Ehmt1* haploinsufficiency leads to abnormal circuit formation and behavioural abnormalities that likely underpin deficits seen across the broad spectrum of neurodevelopmental and neuropsychiatric disorders with which *EHMT1* is associated.

MATERIALS AND METHODS

Animals

All procedures were conducted in accordance with the requirements of the UK Animals (Scientific Procedures) Act 1986, with additional ethical approval at Cardiff University.

In order to generate experimental cohorts, *Ehmt1*$^{flp/flp}$ [22] male studs were paired in trios with one homozygous females carrying two copies of the Tg(Dach1-cre)1Krs/Kctt Cre transgene, maintained on a F1(C57BL/6J x CBA/Ca) background; and one wild-type F1(C57BL/6J x CBA/Ca) female. Experimental cohorts were reared together and then weaned into cages of mixed of *Ehmt1*$^{D6cre/+}$ and control *Ehmt1*$^{Flp/+}$ mice. All experimental subjects were male mice, mixed housed (2-5per cage) and aged between 4-10 months during testing. Standard laboratory diet and water were available *ad libitum* throughout testing.

Experimenters were blind to the genotype of animals during behavioural testing.

Gene Expression

Western blot analysis

Whole head lysates for embryonic stage 12.5 (E12.5) and E13.5 were used; while whole brains were used for E14.5, E18.5, postnatal days 1 (P1) and P7 and P56 in the western blot for peak GLP, G9a and H3K9me2 (Abcam, UK) expression assay. Lysates from ≥4 pups from two separate litters were combined for each time point, except at P56 where two independent whole brain samples were run independently. Tissue was extracted and lysed on ice at 5mg/ml of RIPA buffer (100mM NaCl, 20nM Tris HCl pH 8, 0.5% deoxycholate, 0.5% NP40, 25uL SDS of 20% stock) using a glass dounce homogenizer. Tissue lyses was then agitated for 2h at 4º C. Western Blots were then ran following the 4-12% NuPage protocol.

qPCR

RNA was extracted from macrodissected hippocampi using the RNeasy micro kit (Qiagen) following the manufacturers instructions. A 96 well RT^2 Custom Profiler PCR Array (CAPM12608, Qiagen) for mice was used. The custom genes list was generated based on GLP targets identified in the literature and tissue-specific relevance. For the qPCR array 1µg of total RNA was used and manufacture's instructions were followed, for cDNA synthesis—RT^2 First Strand Kit (Qiagen) and for the RT-PCR reaction—RT^2 SYBR Green ROX qPCR Matermix (Qiagen). The average Ct values across the three housekeeping genes *B2m, B-actin* and *Gapdh*

were used as endogenous controls. ΔCt values were generated by normalizing to the geometric mean of the Ct values for these three housekeeping genes. All individual reactions were carried out in triplicate. Real time qPCR data was visualized using the ΔΔCt method [49].

Behaviour

Behavioural testing was performed in two cohorts as follows. Locomotor activity, elevated plus maze, open field and novelty place preference testing was carried out in N=27 animals (*Ehmt1*$^{Flp/+}$ control mice, n=9; *Ehmt1*$^{D6cre/+}$ mice, n=18). Novel object recognition memory test N=29, (*Ehmt1*$^{Flp/+}$ control mice, n=16; *Ehmt1*$^{D6cre/+}$ mice, n=13). All animals were subject to sensory motor-gating testing (*Ehmt1*$^{Flp/+}$ control mice, n=25; *Ehmt1*$^{D6cre/+}$ mice, n=31).

Locomotor activity

Locomotor activity (LMA) and motoric competence on the rotarod were tested as previously described [50]. Briefly, LMA was measured in custom-built chambers with two infra-red beams crossing each cage 30mm from each end and 10mm from the floor of the chamber. Beam breaks were recorded as an indication of activity, using a computer running custom written BBC Basic V6 programmes with additional interfacing by ARACHNID (Cambridge Cognition Ltd, Cambridge, U.K.). Data stored were the total number of beam-breaks in a 2 hour session. One session was carried out per day, for five consecutive days as a measure of habituation to a novel environment. Habituation to a novel arena was assayed by the decrease in beam breaks between the first and last sessions.

A rotarod task (Ugo Basile, Italy) was used to assess motoric function. Animals received five training sessions. In the test session latency to fall at a set rotating speed was recorded.

Elevated plus maze

The elevated plus maze (EPM) was constructed of black Perspex covered in white tape. The plus shape consisted of two adjacent arms, which were enclosed on the sides (19 x 8 x 15cm, length x width x height) and two adjacent arms, which were open (19 x 8cm, length x width). The maze was 94cm above the ground and illuminated with an even low level white light. All behavior was recored using EthoVision Observer video tracking software (version 3.0.15, Noldus Information Technology, Netherlands) and an overhead digital camera. Animals were placed in the centre of the maze facing one of the open arms and were allowed to explore the maze for 5 min. The EPM

was divided in to 3 virtual zones – open arms, closed arms, middle. Among the variables recored were duration and entries into each zone, time spent moving and rearing frequency.

Open Field

The open field (OF) arena was constructed of white Perspex (75cm x 75cm x 45cm (length x width x height) walls. For analysis purposes, the arena was subdivided into three virtual zones of concentric squares: the inner zone (20 x 20cm), middle zone (40 x 40cm) and outer zone (15cm periphery). All behavior was recorded using EthoVision Observer software. Animals were placed in the arena facing one of the four walls, in the periphery of the arena. Placement was counterbalanced across animals. Among the variables recorded were total time spent in the two central zones, the frequency of entries into the two central zones, the latency of first entry into the Inner zone and the number of rears. Animals were placed in the arena for ten minutes and each session was broken into 1 min intervals to assess performance within a session.

Novelty Place Preference

The novelty place preference (NPP) arena was composed of two perspex chambers each 30cm X 30cm X 30cm (height X width X length) conjoined by a small door. During the habituation phase this door was closed. One chamber had black walls, the other had white. The floor of one chamber was covered in sandpaper in order to increase the valence. The side containing the sandpaper was counterbalanced across genotype and whether received in the habituation and test trial or only the test trial.

Mice were introduced to one chamber, either white or black (counterbalanced across genotype) and allowed to habituate for 60min. Mice were then removed, the arena cleaned thoroughly with 1% acetic acid and the mice returned and allowed to explore the both sides for 30mins. All behaviour was recorded using EthoVision Observer software. The main measurements included the latency to first enter the novel side and the time spent in the novel chamber.

Sensory-motor gating

Acoustic startle response (ASR) and prepulse inhibition (PPI) of the startle response were monitored using a SR-Lab apparatus (San Diego Instruments, U.S.A) modified for use in mice, according to published methods [50]. Briefly, animals were placed in a Perspex tube (internal diameter 35mm) and white noise stimuli were presented via a speaker. Pulse-alone trials consisted of a 40ms startle stimulus and a prepulse trial consisted of a 20ms prepulse at 4, 8, or

16db above background and a 40ms 105db startle stimulus, 70ms after the prepulse. The stimuli were presented in a pseudorandom manner every 15s. Whole body startle responses were recorded as the average startle during a 65ms window timed from the onset of the startle pulse. Response output was adjusted for weight.

Percentage PPI score for each trial was calculated:

[%PPI=100 × (ASRstartle pulse alone − ASRprepulse + startle pulse)/ASRstartle pulse alone].

Novel object recognition memory

The NOR test arena was a square 30cm x 30cm with 30cm high, white Perspex walls. Four different, non-displaceable objects were used. All objects were white and selected for their equal appeal and available in triplicate to avoid the use of olfactory cues. In the habituation phase, 24hr prior to the task, each subject was allowed to explore the arena for 10min in the absence of objects. In the acquisition phase, the subject was returned to the arena containing 2 identical sample objects (A, A') and given 10min to explore. After a retention phase, consisting of 15min or 90min, the subject was returned to the arena with two objects, one identical to the sample and the other novel (A, B). During both the familiarization and test phase, objects were located adjacent corners of the arena. The location of the novel object was counterbalanced. To prevent coercion to explore the objects, the subject was released in a third corner. Objects were cleaned with 70% ethanol wipes between sessions and object selection was randomized.

The Recognition Index (RI) was used as a measure of whether the animal investigated the novel object more than chance. This was calculated by the percentage of time spent investigating the novel object relative to the total object investigation [$RI= T_N/(T_N+T_F) \times 100$]. An RI significantly above chance or 50% indicates recognition of novelty and an RI equal to or below 50% indicates either no preference for the novelty or no recognition of novelty. Other parameters recorded were: frequency and latency to enter the zones containing an object. Data was collected in 1-min time bins across the 10-min session by a camera linked to a computer with Ethovision Observer software (Noldus, Nottingham, UK).

Electrophysiology

Adult male *Ehmt1*$^{D6Cre/+}$ mice (*n*=7) and *Ehmt1*$^{Flp/+}$ control cage-mates (*n*=7) at 6-7 months of age were anesthetized with 2% isoflurane for stereotaxic electrode implantation. The electrode configuration used two bilateral frontal electrodes, one monopolar and one bipolar (2.7-mm

anterior, 1.5-mm lateral, 1.2-deep relative to bregma); two bilateral hippocampal electrodes, one monopolar and one bipolar (2.7 mm posterior, 3-mm lateral, 2.2-mm deep relative to bregma); and one bipolar electrode in the auditory cortex (2.7-mm posterior, 4-mm lateral, 1.1-deep relative to bregma) as has been previously reported [51, 52] (for further details see Supplementary Materials and Methods, and Supplementary Figure 2). Due to animal loss, a subset of these was used in the MMN study; *Ehmt1*$^{D6Cre/+}$ mice (*n*=5) and *Ehmt1*$^{Flp/+}$ control cage-mates (*n*=5).

ERPs were obtained by averaging EEG traces centred at time 0 and 500msec to 0μV, respectively. For each trial, power was calculated by using a complex Morlet's wavelets w(t, f0) [53]. The script used can be found at https://www.physics.lancs.ac.uk/research/nbmphysics/diats/tfr/. The wavelets have a Gaussian shape in the time domain (SD σt) and in the frequency domain (SD σt) around its central frequency *f*0: w(t, f0)=A * exp(-t2/2 σt2) * exp(2iπf0t) with σf=1/πσt. The wavelet family we used was defined by f0/σf=1, with f0 ranging from 0.5 to 100Hz in logarithmically distributed frequency steps (for full details see Supplementary Materials and Methods).

Auditory stimuli were generated using Spike2, version 7.2 and a Power1401 interface (CED, UK). Auditory stimulus was delivered with speakers positioned directly in front of each recording cage. Each mouse received an auditory, paired-pulse session and two sessions of mismatch negativity (MMN).

Paired pulse

Following Halene *et al*. [54], each mouse received an auditory, paired-pulse session in which a single tone was presented at 1500Hz and 90dB (S1) followed by a 500ms intra-trial interval and a second tone at 1500Hz and 90dB (S2). The tones were sinusoidal and 10ms in duration. The inter-pulse interval between the two tones was 10-s. Each mouse received 1250 paired-pulse trials per recording session.

Mismatch negativity

The mice also received two sessions of the MMN protocol. Similar to Ehrlichman *et al*. [51], the mice received 24 'standard' tones at 90dB and 1500Hz and one 'deviant' tone at 90dB and 2000Hz. All tones were sinusoidal and 10ms in duration and the intra-pulse interval between the 25 tones was 500-ms, while the inter-trial interval was 5-s. Each mouse was recorded for 360

trials in each of two sessions. In one session 10mg/kg of Ketamine was administered and in the second session an equal volume of saline was administered. The dosage of ketamine was chosen based on previous work [51, 52]. The within group design was counterbalanced by genotype and the order in which ketamine or saline sessions were administered. All recordings took place 5-mins after intraperitoneal injections of either 10mg/kg ketamine or the volume equivalent dose of saline. The waveform channels were filtered between 1 and 500Hz.

Statistics

All data were analyzed using SPSS 20 (SPSS, USA). The statistical differences between groups were analysed using independent samples t-tests, ANOVAs, or where appropriate Repeated Measures ANOVA (RP-ANOVAs). The main between-subject factor was GENOTYPE ($Ehmt1^{Flp/+}$ controls or $Ehmt1^{D6Cre/+}$). The following within-subject factors were also analysed: DAY (day of testing, LMA and the three days of locomotor learning); time BIN (5-min bins across day one LMA; 5-min bins in NPP); SESSION (locomotor learning); TRIAL (Locomotor coordination); STARTLE and PPI (4, 8 or 16dB); PULSE (standard or deviant in the MMN). To check for normal distribution, Mauchly's test of sphericity of the covariance matrix or Levenes test for equality of variances were applied. The more conservative Huynh-Feldt corrections, with adjusted degrees of freedom are reported in cases in which test assumptions were violated. Non-parametric analyses were as follows. For the NOR task, the binomial distribution one sample Kolmongolov Smirnov (KS) test was applied to determine whether average RIs or SIs were significantly above chance (above 50%). For analysis of N1 amplitude, Wilcoxon sum-rank test was used. Statistical tests on the electrophysiological frequency data were performed using the permutation method with <1,000 iterations [55] (see Supplementary Methods for full details). For all comparisons, alpha value was set at $p<0.05$.

Conflict of interest statement

The authors have no interests in any company or organization that would benefit from this article.

Funding

This work was funded by a Wellcome Trust Integrative Neuroscience PhD grant (WT093765MA) to BAD, AJH and ARI. VC was supported by a Wellcome Trust Programme Grant (91882).

REFERENCES

1. Tyssowski K, Kishi Y, Gotoh Y. Chromatin regulators of neural development. Neuroscience. 2014;264:4-16. doi: 10.1016/j.neuroscience.2013.10.008. PubMed PMID: 24144622.
2. Hirabayashi Y, Gotoh Y. Epigenetic control of neural precursor cell fate during development. Nature reviews Neuroscience. 2010;11(6):377-88. doi: 10.1038/nrn2810. PubMed PMID: 20485363.
3. RK CY, Merico D, Bookman M, J LH, Thiruvahindrapuram B, Patel RV, et al. Whole genome sequencing resource identifies 18 new candidate genes for autism spectrum disorder. Nature neuroscience. 2017. doi: 10.1038/nn.4524. PubMed PMID: 28263302.
4. De Rubeis S, He X, Goldberg AP, Poultney CS, Samocha K, Cicek AE, et al. Synaptic, transcriptional and chromatin genes disrupted in autism. Nature. 2014;515(7526):209-15. doi: 10.1038/nature13772. PubMed PMID: 25363760; PubMed Central PMCID: PMCPMC4402723.
5. Network, Pathway Analysis Subgroup of Psychiatric Genomics C. Psychiatric genome-wide association study analyses implicate neuronal, immune and histone pathways. Nature neuroscience. 2015;18(2):199-209. doi: 10.1038/nn.3922. PubMed PMID: 25599223; PubMed Central PMCID: PMCPMC4378867.
6. Singh T, Kurki MI, Curtis D, Purcell SM, Crooks L, McRae J, et al. Rare loss-of-function variants in SETD1A are associated with schizophrenia and developmental disorders. Nature neuroscience. 2016;19(4):571-7. doi: 10.1038/nn.4267. PubMed PMID: 26974950.
7. Deciphering Developmental Disorders S. Prevalence and architecture of de novo mutations in developmental disorders. Nature. 2017. doi: 10.1038/nature21062. PubMed PMID: 28135719.
8. Talkowski ME, Rosenfeld JA, Blumenthal I, Pillalamarri V, Chiang C, Heilbut A, et al. Sequencing chromosomal abnormalities reveals neurodevelopmental loci that confer risk across diagnostic boundaries. Cell. 2012;149(3):525-37. doi: 10.1016/j.cell.2012.03.028. PubMed PMID: 22521361; PubMed Central PMCID: PMC3340505.
9. Kleefstra T, Brunner HG, Amiel J, Oudakker AR, Nillesen WM, Magee A, et al. Loss-of-function mutations in euchromatin histone methyl transferase 1 (EHMT1) cause the 9q34 subtelomeric deletion syndrome. American journal of human genetics. 2006;79(2):370-7. doi: 10.1086/505693. PubMed PMID: 16826528; PubMed Central PMCID: PMC1559478.
10. Kleefstra T, Smidt M, Banning MJ, Oudakker AR, Van Esch H, de Brouwer AP, et al. Disruption of the gene Euchromatin Histone Methyl Transferase1 (Eu-HMTase1) is associated with the 9q34 subtelomeric deletion syndrome. J Med Genet. 2005;42(4):299-306. doi: 10.1136/jmg.2004.028464. PubMed PMID: 15805155; PubMed Central PMCID: PMCPMC1736026.
11. Cooper GM, Coe BP, Girirajan S, Rosenfeld JA, Vu TH, Baker C, et al. A copy number variation morbidity map of developmental delay. Nature genetics. 2011;43(9):838-46. Epub 2011/08/16. doi: 10.1038/ng.909. PubMed PMID: 21841781; PubMed Central PMCID: PMC3171215.
12. O'Roak BJ, Vives L, Girirajan S, Karakoc E, Krumm N, Coe BP, et al. Sporadic autism exomes reveal a highly interconnected protein network of de novo mutations. Nature. 2012;485(7397):246-50. Epub 2012/04/13. doi: 10.1038/nature10989. PubMed PMID: 22495309; PubMed Central PMCID: PMC3350576.
13. Kirov G, Pocklington AJ, Holmans P, Ivanov D, Ikeda M, Ruderfer D, et al. De novo CNV analysis implicates specific abnormalities of postsynaptic signalling complexes in the

pathogenesis of schizophrenia. Molecular psychiatry. 2012;17(2):142-53. Epub 2011/11/16. doi: 10.1038/mp.2011.154. PubMed PMID: 22083728; PubMed Central PMCID: PMC3603134.
14. Tachibana M, Ueda J, Fukuda M, Takeda N, Ohta T, Iwanari H, et al. Histone methyltransferases G9a and GLP form heteromeric complexes and are both crucial for methylation of euchromatin at H3-K9. Genes & development. 2005;19(7):815-26. doi: 10.1101/gad.1284005. PubMed PMID: 15774718; PubMed Central PMCID: PMC1074319.
15. Gupta-Agarwal S, Franklin AV, Deramus T, Wheelock M, Davis RL, McMahon LL, et al. G9a/GLP histone lysine dimethyltransferase complex activity in the hippocampus and the entorhinal cortex is required for gene activation and silencing during memory consolidation. The Journal of neuroscience : the official journal of the Society for Neuroscience. 2012;32(16):5440-53. doi: 10.1523/JNEUROSCI.0147-12.2012. PubMed PMID: 22514307; PubMed Central PMCID: PMCPMC3332335.
16. Gupta NA, Mells J, Dunham RM, Grakoui A, Handy J, Saxena NK, et al. Glucagon-like peptide-1 receptor is present on human hepatocytes and has a direct role in decreasing hepatic steatosis in vitro by modulating elements of the insulin signaling pathway. Hepatology. 2010;51(5):1584-92. doi: 10.1002/hep.23569. PubMed PMID: 20225248; PubMed Central PMCID: PMCPMC2862093.
17. Heller EA, Cates HM, Pena CJ, Sun H, Shao N, Feng J, et al. Locus-specific epigenetic remodeling controls addiction- and depression-related behaviors. Nature neuroscience. 2014;17(12):1720-7. doi: 10.1038/nn.3871. PubMed PMID: 25347353; PubMed Central PMCID: PMCPMC4241193.
18. Covington HE, 3rd, Maze I, Sun H, Bomze HM, DeMaio KD, Wu EY, et al. A role for repressive histone methylation in cocaine-induced vulnerability to stress. Neuron. 2011;71(4):656-70. doi: 10.1016/j.neuron.2011.06.007. PubMed PMID: 21867882; PubMed Central PMCID: PMCPMC3163060.
19. Maze I, Covington HE, 3rd, Dietz DM, LaPlant Q, Renthal W, Russo SJ, et al. Essential role of the histone methyltransferase G9a in cocaine-induced plasticity. Science. 2010;327(5962):213-6. doi: 10.1126/science.1179438. PubMed PMID: 20056891; PubMed Central PMCID: PMCPMC2820240.
20. Benevento M, Iacono G, Selten M, Ba W, Oudakker A, Frega M, et al. Histone Methylation by the Kleefstra Syndrome Protein EHMT1 Mediates Homeostatic Synaptic Scaling. Neuron. 2016;91(2):341-55. doi: 10.1016/j.neuron.2016.06.003. PubMed PMID: 27373831.
21. Balemans MC, Ansar M, Oudakker AR, van Caam AP, Bakker B, Vitters EL, et al. Reduced Euchromatin histone methyltransferase 1 causes developmental delay, hypotonia, and cranial abnormalities associated with increased bone gene expression in Kleefstra syndrome mice. Developmental biology. 2014;386(2):395-407. doi: 10.1016/j.ydbio.2013.12.016. PubMed PMID: 24362066.
22. Schaefer A, Sampath SC, Intrator A, Min A, Gertler TS, Surmeier DJ, et al. Control of cognition and adaptive behavior by the GLP/G9a epigenetic suppressor complex. Neuron. 2009;64(5):678-91. doi: 10.1016/j.neuron.2009.11.019. PubMed PMID: 20005824; PubMed Central PMCID: PMCPMC2814156.
23. van den Bout CJ, Machon O, Rosok O, Backman M, Krauss S. The mouse enhancer element D6 directs Cre recombinase activity in the neocortex and the hippocampus. Mechanisms of development. 2002;110(1-2):179-82. PubMed PMID: 11744379.

24. Machon O, van den Bout CJ, Backman M, Rosok O, Caubit X, Fromm SH, et al. Forebrain-specific promoter/enhancer D6 derived from the mouse Dach1 gene controls expression in neural stem cells. Neuroscience. 2002;112(4):951-66. PubMed PMID: 12088753.
25. Antunes M, Biala G. The novel object recognition memory: neurobiology, test procedure, and its modifications. Cogn Process. 2012;13(2):93-110. doi: 10.1007/s10339-011-0430-z. PubMed PMID: 22160349; PubMed Central PMCID: PMCPMC3332351.
26. Luck SJ, Mathalon DH, O'Donnell BF, Hamalainen MS, Spencer KM, Javitt DC, et al. A roadmap for the development and validation of event-related potential biomarkers in schizophrenia research. Biological psychiatry. 2011;70(1):28-34. doi: 10.1016/j.biopsych.2010.09.021. PubMed PMID: 21111401; PubMed Central PMCID: PMCPMC3116072.
27. Goffin D, Brodkin ES, Blendy JA, Siegel SJ, Zhou Z. Cellular origins of auditory event-related potential deficits in Rett syndrome. Nature neuroscience. 2014;17(6):804-6. doi: 10.1038/nn.3710. PubMed PMID: 24777420; PubMed Central PMCID: PMCPMC4038660.
28. Roach BJ, Mathalon DH. Event-related EEG time-frequency analysis: an overview of measures and an analysis of early gamma band phase locking in schizophrenia. Schizophrenia bulletin. 2008;34(5):907-26. doi: 10.1093/schbul/sbn093. PubMed PMID: 18684772; PubMed Central PMCID: PMCPMC2632478.
29. Light GA, Braff DL. Stability of mismatch negativity deficits and their relationship to functional impairments in chronic schizophrenia. The American journal of psychiatry. 2005;162(9):1741-3. doi: 10.1176/appi.ajp.162.9.1741. PubMed PMID: 16135637.
30. Sivarao DV, Chen P, Yang Y, Li YW, Pieschl R, Ahlijanian MK. NR2B Antagonist CP-101,606 Abolishes Pitch-Mediated Deviance Detection in Awake Rats. Front Psychiatry. 2014;5:96. doi: 10.3389/fpsyt.2014.00096. PubMed PMID: 25140157; PubMed Central PMCID: PMCPMC4122188.
31. Umbricht D, Koller R, Vollenweider FX, Schmid L. Mismatch negativity predicts psychotic experiences induced by NMDA receptor antagonist in healthy volunteers. Biological psychiatry. 2002;51(5):400-6. PubMed PMID: 11904134.
32. Dawson GR, Tricklebank MD. Use of the elevated plus maze in the search for novel anxiolytic agents. Trends Pharmacol Sci. 1995;16(2):33-6.
33. Balemans MC, Huibers MM, Eikelenboom NW, Kuipers AJ, van Summeren RC, Pijpers MM, et al. Reduced exploration, increased anxiety, and altered social behavior: Autistic-like features of euchromatin histone methyltransferase 1 heterozygous knockout mice. Behavioural brain research. 2010;208(1):47-55. Epub 2009/11/10. doi: 10.1016/j.bbr.2009.11.008. PubMed PMID: 19896504.
34. Javitt DC. Sensory processing in schizophrenia: neither simple nor intact. Schizophrenia bulletin. 2009;35(6):1059-64. doi: 10.1093/schbul/sbp110. PubMed PMID: 19833806; PubMed Central PMCID: PMCPMC2762632.
35. Orekhova EV, Stroganova TA, Prokofyev AO, Nygren G, Gillberg C, Elam M. Sensory gating in young children with autism: relation to age, IQ, and EEG gamma oscillations. Neuroscience letters. 2008;434(2):218-23. doi: 10.1016/j.neulet.2008.01.066. PubMed PMID: 18313850.
36. Perry W, Minassian A, Lopez B, Maron L, Lincoln A. Sensorimotor gating deficits in adults with autism. Biological psychiatry. 2007;61(4):482-6. doi: 10.1016/j.biopsych.2005.09.025. PubMed PMID: 16460695.

37. Belmonte MK, Cook EH, Jr., Anderson GM, Rubenstein JL, Greenough WT, Beckel-Mitchener A, et al. Autism as a disorder of neural information processing: directions for research and targets for therapy. Molecular psychiatry. 2004;9(7):646-63. doi: 10.1038/sj.mp.4001499. PubMed PMID: 15037868.
38. Kwon JS, O'Donnell BF, Wallenstein GV, Greene RW, Hirayasu Y, Nestor PG, et al. Gamma frequency-range abnormalities to auditory stimulation in schizophrenia. Archives of general psychiatry. 1999;56(11):1001-5. PubMed PMID: 10565499; PubMed Central PMCID: PMCPMC2863027.
39. Tatard-Leitman VM, Jutzeler CR, Suh J, Saunders JA, Billingslea EN, Morita S, et al. Pyramidal cell selective ablation of N-methyl-D-aspartate receptor 1 causes increase in cellular and network excitability. Biological psychiatry. 2015;77(6):556-68. doi: 10.1016/j.biopsych.2014.06.026. PubMed PMID: 25156700; PubMed Central PMCID: PMCPMC4297754.
40. Iaccarino HF, Singer AC, Martorell AJ, Rudenko A, Gao F, Gillingham TZ, et al. Gamma frequency entrainment attenuates amyloid load and modifies microglia. Nature. 2016;540(7632):230-5. doi: 10.1038/nature20587. PubMed PMID: 27929004.
41. Cardin JA, Carlen M, Meletis K, Knoblich U, Zhang F, Deisseroth K, et al. Driving fast-spiking cells induces gamma rhythm and controls sensory responses. Nature. 2009;459(7247):663-7. doi: 10.1038/nature08002. PubMed PMID: 19396156; PubMed Central PMCID: PMCPMC3655711.
42. Roy DS, Arons A, Mitchell TI, Pignatelli M, Ryan TJ, Tonegawa S. Memory retrieval by activating engram cells in mouse models of early Alzheimer's disease. Nature. 2016;531(7595):508-12. doi: 10.1038/nature17172. PubMed PMID: 26982728; PubMed Central PMCID: PMCPMC4847731.
43. Fries P. Rhythms for Cognition: Communication through Coherence. Neuron. 2015;88(1):220-35. doi: 10.1016/j.neuron.2015.09.034. PubMed PMID: 26447583; PubMed Central PMCID: PMCPMC4605134.
44. Furuse T, Wada Y, Hattori K, Yamada I, Kushida T, Shibukawa Y, et al. Phenotypic characterization of a new Grin1 mutant mouse generated by ENU mutagenesis. The European journal of neuroscience. 2010;31(7):1281-91. doi: 10.1111/j.1460-9568.2010.07164.x. PubMed PMID: 20345915.
45. Mohn AR, Gainetdinov RR, Caron MG, Koller BH. Mice with reduced NMDA receptor expression display behaviors related to schizophrenia. Cell. 1999;98(4):427-36. PubMed PMID: 10481908.
46. Duncan GE, Moy SS, Perez A, Eddy DM, Zinzow WM, Lieberman JA, et al. Deficits in sensorimotor gating and tests of social behavior in a genetic model of reduced NMDA receptor function. Behavioural brain research. 2004;153(2):507-19. doi: 10.1016/j.bbr.2004.01.008. PubMed PMID: 15265649.
47. Featherstone RE, Shin R, Kogan JH, Liang Y, Matsumoto M, Siegel SJ. Mice with subtle reduction of NMDA NR1 receptor subunit expression have a selective decrease in mismatch negativity: Implications for schizophrenia prodromal population. Neurobiology of disease. 2015;73:289-95. doi: 10.1016/j.nbd.2014.10.010. PubMed PMID: 25461194.
48. Gandal MJ, Sisti J, Klook K, Ortinski PI, Leitman V, Liang Y, et al. GABAB-mediated rescue of altered excitatory-inhibitory balance, gamma synchrony and behavioral deficits following constitutive NMDAR-hypofunction. Transl Psychiatry. 2012;2:e142. doi: 10.1038/tp.2012.69. PubMed PMID: 22806213; PubMed Central PMCID: PMCPMC3410621.

49. Livak KJ, Schmittgen TD. Analysis of relative gene expression data using real-time quantitative PCR and the 2(-Delta Delta C(T)) Method. Methods. 2001;25(4):402-8. PubMed PMID: 11846609.
50. McNamara GI, Davis BA, Dwyer DM, John RM, Isles AR. Behavioural abnormalities in a novel mouse model for Silver Russell Syndrome. Human molecular genetics. 2016;25(24):5407-17. doi: 10.1093/hmg/ddw357. PubMed PMID: 27798108.
51. Ehrlichman RS, Maxwell CR, Majumdar S, Siegel SJ. Deviance-elicited changes in event-related potentials are attenuated by ketamine in mice. J Cogn Neurosci. 2008;20(8):1403-14. doi: 10.1162/jocn.2008.20097. PubMed PMID: 18303985.
52. Siegel SJ, Connolly P, Liang Y, Lenox RH, Gur RE, Bilker WB, et al. Effects of strain, novelty, and NMDA blockade on auditory-evoked potentials in mice. Neuropsychopharmacology : official publication of the American College of Neuropsychopharmacology. 2003;28(4):675-82. doi: 10.1038/sj.npp.1300087. PubMed PMID: 12655312.
53. Kronland-Martinet R, Morlet J, Grossmann A. Analysis of sound patterns through wavelet transforms. International journal of pattern recognition and artificial intelligence. 1987;1(02):273-302. doi: 10.1142/S0218001487000205.
54. Halene TB, Ehrlichman RS, Liang Y, Christian EP, Jonak GJ, Gur TL, et al. Assessment of NMDA receptor NR1 subunit hypofunction in mice as a model for schizophrenia. Genes, brain, and behavior. 2009;8(7):661-75. doi: 10.1111/j.1601-183X.2009.00504.x. PubMed PMID: 19563516; PubMed Central PMCID: PMCPMC2757454.
55. Westfall PH, Young SS. Resampling-based multiple testing: Examples and methods for p-vlaue adjustment. New York: Wiley; 1993.